

# Faraday rotation of the supernova remnant G296.5+10.0: Evidence for a Magnetized Progenitor Wind

L. Harvey-Smith,<sup>1</sup> B. M. Gaensler,<sup>1,5</sup> R. Kothes,<sup>2</sup> R. Townsend,<sup>3</sup> G. H. Heald,<sup>4</sup> C.-Y. Ng<sup>1</sup>  
and A. J. Green<sup>1</sup>

## ABSTRACT

We present spectropolarimetric radio images of the supernova remnant (SNR) G296.5+10.0 at frequencies near 1.4 GHz, observed with the Australia Telescope Compact Array. By applying rotation measure (RM) synthesis to the data, a pixel-by-pixel map of Faraday rotation has been produced for the entire remnant. We find G296.5+10.0 to have a highly ordered RM structure, with mainly positive RMs (mean RM of  $+28 \text{ rad m}^{-2}$ ) on the eastern side and negative RMs (mean RM of  $-14 \text{ rad m}^{-2}$ ) on the western side, indicating a magnetic field which is directed away from us on one side and toward us on the other. We consider several possible mechanisms for creating the observed RM pattern. Neither Faraday rotation in foreground interstellar gas nor in a homogeneous ambient medium swept up by the SNR shell can easily explain the magnitude and sign of the observed RM pattern. Instead, we propose that the observed RMs are the imprint of an azimuthal magnetic field in the stellar wind of the progenitor star. Specifically, we calculate that a swept-up magnetized wind from a red supergiant can produce RMs of the observed magnitude, while the azimuthal pattern of the magnetic field at large distances from the star naturally produces the anti-symmetric RM pattern observed. Expansion into such a wind can possibly also account for the striking bilateral symmetry of the SNR's radio and X-ray morphologies.

*Subject headings:* ISM: individual (G296.5+10.0), magnetic fields — polarization — stars: winds — supernova remnants — radio continuum: ISM

---

<sup>1</sup>Sydney Institute for Astronomy (SIfA), School of Physics, The University of Sydney, NSW 2006, Australia; lhs@usyd.edu.au

<sup>2</sup>National Research Council of Canada, Herzberg Institute of Astrophysics, Dominion Radio Astrophysical Observatory, Penticton, British Columbia, V2A 6J9, Canada

<sup>3</sup>Department of Astronomy, University of Wisconsin, Madison, WI 53706

<sup>4</sup>ASTRON, 7990 AA Dwingeloo, The Netherlands

<sup>5</sup>Federation Fellow, Australian Research Council

## 1. Introduction

Observations of radio supernova remnants (SNRs) provide a unique probe of the circumstellar environments of supernova progenitor stars and the interstellar medium (ISM). In particular, the interactions between SNRs and their environments give rise to a wide range of observable effects from which we can derive important physical insights. Spectral line maps of neutral hydrogen (HI) in the vicinity of SNRs enable us to calculate the age, swept-up shell mass and energy of the supernova explosion (Gaensler et al. 1998; Velázquez et al. 2002; Foster et al. 2004). Combined with model rotation curves for the Galaxy, HI data may be used to constrain the kinematic distance to the remnant (Pineault et al. 1993; Tian & Leahy 2008). Under certain conditions, regions of interaction between a SNR shock and a dense molecular cloud produce hydroxyl masers, allowing us to derive the properties of the SNR shock, estimate the distance to the remnant and to calculate the postshock magnetic field through the Zeeman effect (Frail et al. 1994; Claussen et al. 1997). In many SNRs there is evidence of physical confinement by denser, cooler surrounding material, which allows us to probe the physical, chemical and magnetic properties of molecular clouds (Burton et al. 1988; Frail et al. 1994; Green et al. 1997; Chevalier 1999) and provide information on particle acceleration and the production of cosmic rays (e.g., Koyama et al. 1995; Tanimori et al. 1998; Fukui et al. 2003).

The appearance of young SNRs can be strongly influenced by the mass-loss history of the progenitor star (Chevalier 1982; Franco et al. 1991; Koo & Heiles 1995). For example, the properties of the progenitor stellar wind have been inferred in the young SNR Cassiopeia A by studying the dynamics of the clumpy shock boundary in the remnant and calculating the swept-up shell mass (Chevalier & Oishi 2003; Vink et al. 1998). In addition, the structure and brightness evolution of the radio remnant of supernova 1987A has been shown to have been shaped by successive interactions of the remnant with material from stellar winds originating from the blue- and red-supergiant phases of the progenitor star (Chevalier & Fransson 1987; Gaensler et al. 1997). Interaction of the supernova ejecta with stellar winds is a phenomenon that occurs in the earlier or mid-stages of a radio SNR’s life (Dwarkadas 2005) although in some cases the passage of the remnant through the circumstellar material (CSM) can continue for many thousands of years in large stellar wind bubbles (Landecker et al. 1999; Gvaramadze 2006).

Magnetic fields are known to influence the development of supernova remnants (Kulsrud et al. 1965; Chevalier 1974). This can be as a direct consequence of magnetic confinement of the expanding SNR shell under the influence of external ISM magnetic fields (van der Laan 1962a; Whiteoak & Gardner 1968), or due to the sweeping-up of a CSM whose distribution is already anisotropic due to magnetic channeling and confinement of the pre-supernova wind(s)

(see, e.g., ud-Doula & Owocki 2002; ud-Doula et al. 2008).

Alternatives to the direct shaping of SNRs by magnetic confinement have also been proposed. Bisnovaty-Kogan et al. (1990) asserted that the eventual shape of a supernova remnant is primarily influenced by the shape of the cavity swept out by the progenitor star. In some cases, the shape of such a stellar wind bubble will be dominated by magnetic fields. In a theoretical treatment of this problem, Chevalier & Luo (1994) considered the case of a bubble driven by a magnetized stellar wind. They found that, in a bubble resulting from a stellar wind with a toroidal magnetic field, the magnetic tension in the equatorial region of the shell can confine the bubble and cause elongation in the polar direction. The proposal that SNRs can be shaped by a magnetically-influenced cavity was arrived at by Gaensler (1998), who proposed that SNRs with barrel morphologies (remnants with negligible emission along the axis of symmetry and bright limbs of emission perpendicular to this axis) form in ISM bubbles that are elongated by the Galactic magnetic field. Whether this elongation is due directly to magnetic confinement or the product of density stratifications along the local magnetic field axis is less clear.

All of these different mechanisms will have an effect at some point in the life of a SNR. It is likely that very young remnants are dominated by the supernova explosion itself, middle-aged remnants will primarily be sculpted by the CSM and older remnants will be shaped by the surrounding ISM. Disentangling these different effects is a complicated task, but if the production and evolution of supernova remnants is to be understood, quantitative studies of the magnetic fields in their immediate environments are crucial.

A useful experimental probe of cosmic magnetic fields is Faraday rotation. When polarized electromagnetic radiation propagates through a magnetized ionized medium, its electric field vector is rotated through an angle which depends on the square of the wavelength and the path integral of the electron-weighted line-of-sight magnetic field strength. This effect is called Faraday rotation. The angle of rotation,  $\Delta\chi$ , is related to the square of the wavelength,  $\lambda$ , via  $\Delta\chi = RM\lambda^2$  where the RM is the rotation measure and is defined as

$$\text{RM} = 0.81 \int_{\text{source}}^{\text{observer}} n_e B_{\parallel} dl \text{ rad m}^{-2} \quad (1)$$

where  $B_{\parallel}$  is the line-of-sight component of the magnetic field strength in  $\mu\text{G}$ ,  $n_e$  is the electron density in  $\text{cm}^{-3}$  and  $dl$  is measured in parsecs.

Evaluating the RM of linearly polarized radio emission gives us an indication of the line-of-sight magnetic field orientation in the foreground Faraday rotating medium. Measurements of other physical cues, such as the interstellar rotation measure along similar lines

of sight, can assist us in disentangling the Faraday rotation due to the Galactic foreground from the RM occurring internally to the source being studied. If the RM is intrinsic to the source, by measuring RMs at many points in an image we can learn about the line-of-sight orientation of the smooth component of the magnetic field in that source. In a supernova remnant, this will either tell us about the ambient magnetic field in the ISM, or the magnetic field in the swept-up shell of circumstellar material depending on the age and history of the remnant.

In this paper we consider the Faraday rotation against G296.5+10.0 (also known as PKS 1209–51/52), a high-Galactic latitude supernova remnant with a barrel morphology at both radio and X-ray wavelengths (Whiteoak & Gardner 1968; Roger et al. 1988; Helfand & Becker 1984). The limbs of the remnant are believed to mark the material swept up by the blast wave from a core-collapse supernova as evidenced by the radio-quiet X-ray emitting neutron star (1E 1207.4–5209) at its center (Helfand & Becker 1984; Zavlin et al. 2000, 2004). G296.5+10.0 displays a high degree of reflection symmetry (Storey et al. 1992), and lies 10 degrees above the Galactic plane at an estimated distance of 2.1 kpc (Giacani et al. 2000).

Attempts to measure the polarization and rotation measure in G296.5+10.0 have previously been made by Whiteoak & Gardner (1968); Dickel & Milne (1976) and Milne & Haynes (1994), but these were limited in their accuracy because the RMs were derived by a linear fit to only two or three points in a plot of position angle vs.  $\lambda^2$ . This method of determining RMs introduces significant uncertainties into the quoted values, because the polarization position angle is known only as a multiplicative factor of  $n\pi$  radians. By using rotation measure synthesis (Brentjens & de Bruyn 2005) to produce a well-sampled rotation measure spectrum at each image pixel, it is possible to eliminate these ambiguities and determine accurate RMs for the entire region. Another advantage of RM synthesis is that it allows us to resolve multiple RM components within a single line of sight. With the flexible correlator on the Australia Telescope Compact Array (ATCA) this can be achieved within a single 128 MHz frequency band.

In this paper, we present full polarization and rotation measure synthesis images of G296.5+10.0 using RM synthesis of ATCA data. In §2 we introduce the observations and methods of data analysis and in §3 we show total intensity, polarization and rotation measure images and plots of RM distribution in G296.5+10.0. The RM distribution and magnetic fields in G296.5+10.0 are discussed in §4. §5 describes our conclusions and suggestions for future work in this field.

## 2. Observations & Analysis

The supernova remnant G296.5+10.0 was observed between the 8th and the 11th of October 1998 using the ATCA. Analysis of the HI data from these observations was published by Giacani et al. (2000). We obtained the data from the ATCA archive in order to extract and analyze the (as yet unpublished) commensally recorded multi-channel continuum polarization information. The observations were carried out in the 210 m configuration, resulting in an angular resolution of  $1'.5$  at the central frequency of 1384 MHz. The total bandwidth of 128 MHz was correlated in  $32 \times 4$  MHz overlapping spectral channels. Those channels affected by self-interference, edge channels and overlapping channels were discarded to leave a useable bandwidth of 104 MHz split into  $13 \times 8$  MHz channels. Calibration terms were determined using observations of the sources PKS 1215-457 (gain solutions) and PKS 1934-638 (flux, polarization leakage and bandpass solutions) using the software reduction package MIRIAD (Sault & Killeen 2004). 109 individual pointings were combined to produce mosaiced images of the entire remnant in Stokes- $I, Q, U, V$  and polarized intensity. Images were deconvolved using the maximum entropy method using the MIRIAD task PMOSMEM (Sault et al. 1999). The RMS noise levels in the final continuum images were 2.0, 1.1 and 1.2 mJy beam $^{-1}$  for Stokes- $I, Q$  and  $U$  respectively. In order to make RM synthesis images, we also made separate mosaic images of each individual spectral channel for Stokes- $Q$  and  $U$ , which had mean RMS noise levels of 3.4 and 3.5 mJy beam $^{-1}$ , respectively. The maximum angular scale to which an interferometer is sensitive is set by the shortest spacing between antennas, in this case 31 metres. As a result, any emission greater than  $24'$  is not detected in our ATCA observations, resulting in a Stokes- $I$  flux on large scales below the true value. Polarization images of the region are likely to contain almost all the flux however, as differential Faraday rotation in the Galactic foreground is expected to break the polarized image into smaller-scale structures.

Rotation measure synthesis (Brentjens & de Bruyn 2005) was employed to produce a full RM spectrum for each image pixel in steps of  $20 \text{ rad m}^{-2}$  between  $-2000$  and  $+2000 \text{ rad m}^{-2}$ . The RM function had a FWHM of  $530 \text{ rad m}^{-2}$ . We then used the spectral deconvolution algorithm RMCLEAN (Heald et al. 2009) with a maximum of 1000 iterations and a CLEAN cutoff of 0.0001 to remove the sidelobe pattern resulting from incomplete  $\lambda^2$  sampling. The outcome of these procedures was a spectrum of polarized flux as a function of RM at each pixel, with typical signal-to-noise ratio of  $\sim 30$  and a median RM uncertainty of  $5.5 \text{ rad m}^{-2}$ . Finally, an image of polarized intensity across the remnant was generated by using a 3-point polynomial fit around the peak of the deconvolved rotation measure spectrum at each pixel. Although we are able to confidently detect a polarized signal at a signal-to-noise ratio of  $\sim 4 - 5$ , a meaningful RM can only be extracted for a somewhat stronger signal (Brentjens & de Bruyn 2005). Accordingly, regions of the final polarized image with

a signal below  $10 \times$  the root mean squared noise level in that image were masked (excluded) from the final maps of RM and polarization. At these high thresholds, polarization bias is negligible and so no debiasing was applied to any of the data.

### 3. Results

Figure 1 presents the images of (a) total intensity, (b) total polarized intensity (the peak  $P$  as a function of RM in the RM synthesis spectrum) and (c) & (d) peak rotation measure for SNR G296.5+10.0. We see a clear bilateral morphology in both the total intensity and the polarized intensity images, with bright limbs of emission to the east and west of the SNR symmetry axis. Along this axis, there appears to be a complete absence of radio emission. The mean fractional polarization of G296.5+10.0, found by comparing the flux density of the total polarized intensity and the Stokes- $I$  images at each pixel, is approximately 35%. This is likely an upper limit, as our observations are not sensitive to large-scale total power emission, as discussed in §2. Figure 1 (c) shows the rotation measures as boxes, denoting the RM value averaged over five adjacent pixels. Filled boxes, representing positive RMs, dominate the eastern limb and unfilled boxes (negative RMs) dominate the western limb of the remnant. Figure 1 (d) shows the same information as an image. Figure 2 shows a typical rotation measure spectrum for a pixel in each of the eastern and western limbs of G296.5+10.0. The polarized flux density is similar in each limb of the SNR, but the RM changes from positive to negative on either side of the symmetry axis.

In order to quantify the distributions of rotation measures in G296.5+10.0 in Figure 3 we plot RM against Right Ascension (upper panel) and against Declination (lower panel). In both plots, the mean RM in each limb is displayed as a dashed line. The upper panel of Figure 3 shows a jump in RM distribution between the limbs of the SNR. The western limb has a mean RM of  $-14 \pm 80$  rad m<sup>-2</sup> and the eastern limb has a mean of  $+28 \pm 65$  rad m<sup>-2</sup>. In contrast, in the lower panel of Figure 3 we see no such gradient or discontinuity in RM as a function of declination. This observation is crucial to our understanding of the magnetic field in the region, which we discuss further in §§4.2, 4.3 and 4.4.

## 4. Discussion

### 4.1. Comparison with previous results

The distribution of RM in Figure 1 along the limbs of G296.5+10.0 has a clear symmetry: the eastern limb shows predominantly positive RMs, while the western limb displays negative

RMs. Since the sign of the RM corresponds to the direction of the electron-weighted average magnetic field between the observer and the source of emission, our results provide a high-angular resolution view of the orientation of the magnetic field responsible for the Faraday rotation. Specifically, the average magnetic field vector points generally toward from us on the eastern side, and away from us on the western side.

We first compare our results to previous studies of polarization and Faraday rotation toward SNR G296.5+10.0. Whiteoak & Gardner (1968) first studied the magnetic fields in G296.5+10.0 using the Parkes 64-m radio telescope to map polarized radio continuum emission from the remnant at 0.6, 1.4 and 2.7 GHz. They made maps of RM across the source by measuring the best-fit linear relationship between the polarization angle and the square of the wavelength at each image pixel. The resulting RM map showed a positive range of RMs (+17 to +36 rad m<sup>-2</sup>) in the eastern limb with a positive gradient of RM with increasing declination. In the western limb, they found a spread of negative (−4 to −14 rad m<sup>-2</sup>) RMs with no declination dependence. Dickel & Milne (1976) used a similar method to compare the polarized radio continuum emission at 2.7 and 5.0 GHz. They noted that the remnant has a moderate east-west RM gradient and that the projected magnetic field has an orientation that runs tangential to the bright edges of the SNR. They also measured an east-west gradient in rotation measure of +38 to −18 rad m<sup>-2</sup> with uncertainties of ±23 rad m<sup>-2</sup>, which agree with the values found by Whiteoak & Gardner (1968). Milne & Haynes (1994) observed G296.5+10.0 using the Parkes 64-m telescope at 2.4, 4.8 and 8.4 GHz. This study surpassed the two previous polarization observations of the region, having both a higher frequency and angular resolution than measured previously. They too found strong evidence for a tangential plane of sky magnetic field. Their RM maps indicated largely negative RMs across the majority of the remnant, but with a large patch of positive RM values around the middle of the eastern limb.

Our results agree broadly with the east-west gradient of RMs found by Whiteoak & Gardner (1968) and Dickel & Milne (1976), although we find no evidence for a declination dependence of RM in the eastern limb. However, our RMs are not readily compared with those derived by Milne & Haynes (1994); they quote a much higher range of RMs. This may be in some part due to their cutoff level for rotation measures being 5% of the peak polarized flux at that frequency, which is a much less stringent cutoff criterion than our 10 $\sigma$  in the peak polarized intensity. The upper limit on percentage polarization we derive (35%) broadly agrees with that (“in excess of 30%”) quoted by Milne & Haynes (1994). Our data were taken around 1.4 GHz, a low radio frequency where extrapolation of measured polarization angles to intrinsic values would give large (> 1 radian) uncertainties. We do not provide such extrapolations here and assume the tangential distribution of intrinsic projected magnetic field vectors calculated by previous authors.

Before we interpret the polarization information gained from our observations, we need to consider whether the observed Faraday rotation is predominantly occurring in unrelated foreground interstellar gas (e.g., Caswell et al. 2004), or in material that has been swept up by the expanding SNR (Matsui et al. 1984; Kothes & Brown 2009).

#### 4.2. The RM of the Foreground ISM

Radio pulsars are typically strongly linearly polarized, and consequently many such sources in the ATNF Pulsar Catalogue<sup>1</sup> (Manchester et al. 2005) have measured RMs. Pulsars are at a variety of distances within the Galaxy, and their Faraday rotation is thought to have no intrinsic component due to the pulsar itself. We can thus compare the RMs seen against G296.5+10.0 to the RMs of pulsars in a similar direction and at comparable distances, to assess whether the RMs seen toward G296.5+10.0 are due to the foreground ISM.

There are two pulsars in the catalogue which sit within  $10^\circ$  of G296.5+10.0, and have estimated distances between 1 and 3 kpc (bracketing the distance to the SNR): PSR B1133–55 ( $\ell = 292:3$ ,  $b = +5:9$ ) has  $\text{RM} = +28 \pm 5 \text{ rad m}^{-2}$  at a distance of  $\approx 2.6$  kpc (Qiao et al. 1995) while PSR J1253–5820 ( $\ell = 303:2$ ,  $b = +4:5$ ) has  $\text{RM} = +18 \pm 1 \text{ rad m}^{-2}$  at a distance  $\approx 2.9$  kpc (Noutsos et al. 2008), where the distance estimates come from the NE2001 Galactic electron density of Cordes & Lazio (2002). If we assume that the observed RM is the projection of a magnetic field predominantly parallel to the Galactic plane, and that the field is sufficiently uniform along these sightlines that the magnitude of the RM scales with distance, we can estimate from this pulsar data that the RM of the foreground ISM between Earth and the SNR is approximately +10 to +20  $\text{rad m}^{-2}$ .

We do not find a good match between this expectation and the observed distribution of RMs against the SNR. The RMs of the western limb are of the opposite sign to the pulsar RMs, while those in the east are of the correct sign, but typically have a magnitude twice as large as what would be expected from the pulsar data.

Additional evidence against a foreground interpretation for the SNR RMs is the relative uniformity of the sign of the RM distribution along each limb (shown in the lower panel of Figure 3), but the difference in the sign of RM between limbs (upper panel of Figure 3). If this Faraday rotation occurs in the foreground, it requires a complete reversal of the magnetic field on a relatively small scale in the east-west direction, but no such reversals along

---

<sup>1</sup>On-line catalogue at <http://www.atnf.csiro.au/research/pulsar/psrcat>



a north-south axis. This situation must be reasonably localized, because no such reversal is seen in the RMs of pulsars or of extragalactic sources at the same Galactic longitude but at lower Galactic latitudes (Brown et al. 2007). While such “magnetic anomalies” have been seen previously in RM (e.g., Brown & Taylor 2001), they tend to be associated with the complicated distribution of ionized gas and magnetic fields along the Galactic plane. At this relatively high Galactic latitude, with no other extended sources or features anywhere in the vicinity, it is hard to see what could cause the required foreground RM distribution. It would also need to be a convenient coincidence that the RM distribution of an unrelated foreground feature has a symmetry axis that aligns with that defined by the SNR’s morphology. We conclude that the RM pattern seen against G296.5+10.0 is most likely intrinsic to the source, and must therefore result from material swept by the expansion of the SNR into its surroundings.

### 4.3. The RM of a Swept-Up Uniform Ambient Medium

Kothes & Brown (2009) have pointed out that ambient gas swept up into a shell by an expanding SNR can produce an observable RM signal, and that the resulting systematic variations in RM as a function of position around the SNR can be used to infer the *in situ* magnetic field geometry of the gas into which the SNR has exploded. However, there are two difficulties arising if the RMs seen toward G296.5+10.0 are interpreted in this way.

First, the observed pattern of RMs is completely contrary to expectations. If a SNR expands into a well-ordered ambient field with a significant component in the plane of the sky, a barrel morphology should result as is observed here (van der Laan 1962b; Whiteoak & Gardner 1968), but there will be identical RM gradients along each SNR limb, with the gradient aligned with the SNR’s symmetry axis (Kothes & Brown 2009). We observe the exact opposite here: there is a minimal RM gradient along the SNR’s symmetry axis, but a large gradient across it (Figure 3). This field geometry is difficult to explain by a model in which the SNR sweeps up a uniform magnetic field.

Second, the magnitude of the RM through the shell implied by this scenario is much larger than observed. To illustrate this, we assume that the RM pattern of the SNR is due to a geometric effect that is occurring equally in both limbs (deferring a specific interpretation of this pattern until §4.4 below). We then compare the RMs of the two limbs to separate the foreground RM contribution from that due to material in the SNR shell: the average RM between the two limbs is approximately +5 to +10 rad m<sup>-2</sup> (which is roughly consistent with the foreground contribution estimated in §4.2 above), while the difference between the limbs is  $\approx 40$  rad m<sup>-2</sup>. Thus we estimate that the observed RM contribution of each limb is

$\approx 20 \text{ rad m}^{-2}$ , with the average field directed in opposite directions on each side to produce the observed RM pattern.

Assuming that the synchrotron-emitting and Faraday-rotating regions in the swept-up shell are mixed together, the region will not be Faraday thin, but rather will emit a continuous spread of superimposed RMs, ranging from a foreground-only RM from material at the edge of the SNR closest to Earth to a maximal RM value experienced by polarized signals that propagate from the back of the SNR, through the swept-up shell, and then through the foreground ISM. The observed RMs and the variation between them are both much smaller than the width of the RM transfer function in our observations of  $\sim 500 \text{ rad m}^{-2}$ . We thus cannot resolve the source as Faraday thick, but instead will measure an average RM equal to half the full value through the SNR (Gardner & Whiteoak 1966; Sokoloff et al. 1998). Thus in relating the observations to the electron density and magnetic field strength in the swept-up limbs, the observed RM of  $\approx 20 \text{ rad m}^{-2}$  implies an RM through the SNR shell of  $\text{RM}_{\text{ISM}} \approx 40 \text{ rad m}^{-2}$ .

To compare this to the expected value of  $\text{RM}_{\text{ISM}}$ , we assume that a SNR of radius  $R$  pc has expanded into a medium of uniform hydrogen density  $n_0 \text{ cm}^{-3}$ . If the SNR shock compresses the material that it sweeps up by a factor  $X$ , then the thermal electron density within the material shocked by the SNR (assuming 100% ionization of ambient gas by the SNR shock) is  $n_1 = Xn_0$  where the subscript 1 denotes the post-shock state. Conservation of mass requires that the thickness of the swept-up shell is  $\Delta R = R/3X$ , while the maximum depth of a sightline through the SNR limb is  $L \approx 2(2R\Delta R)^{1/2}$  (assuming  $\Delta R \ll R$ ). The RM through the entire limb is then  $0.81n_1B_1L \cos \theta$ , where  $B_1$  is the magnetic field strength in the post-shock gas, and  $\theta$  is the angle of the post-shock field to the line of sight. The maximal RM for the swept-up material, for  $\theta = 0$ , is then  $\text{RM}_{\text{ISM}} \approx 1.3X^{1/2}n_0B_1R \text{ rad m}^{-2}$ .

At a distance of 2.1 kpc, a representative radius for the SNR (measured from the geometric center to the brightest regions of the limbs to the east and west) is  $R \approx 20$  pc. HI and X-ray observations of the SNR imply  $n_0 \sim 0.1 \text{ cm}^{-3}$  (Dubner et al. 1986; Matsui et al. 1988), while equipartition between relativistic particles and magnetic fields in the emitting region (e.g., Pacholczyk 1970) implies strength in the SNR shell of  $B_1 \approx 25 - 50 \mu\text{G}$ . Roger et al. (1988) argue that SNR G296.5+10.0 is in the adiabatic (Sedov-Taylor) phase of evolution, for which  $X = 4$ ; the implied shell thickness  $\Delta R = R/12$  is consistent with the observed SNR morphology. We then predict  $\text{RM}_{\text{ISM}} \approx 130 - 260 \text{ rad m}^{-2}$ , which is substantially larger than the value  $\text{RM}_{\text{ISM}} \approx 40 \text{ rad m}^{-2}$  required by observations. From the above considerations, we conclude that an ambient uniform medium cannot explain either the strength or pattern of the observed RMs.

#### 4.4. The RM of the Swept-Up Progenitor Wind

An alternative explanation for the RMs observed in G296.5+10.0 is Faraday rotation through the magneto-ionic medium of the swept-up stellar wind from the supernova progenitor. At large distances from the stellar surface, stellar winds are expected to have largely toroidal fields; if such a field geometry is preserved after material has been swept up by the supernova explosion, this could potentially produce an RM pattern that was negative on one limb of the SNR and positive on the other. We now consider this possibility in detail.

The presence of a central neutron star in G296.5+10.0 (e.g., Helfand & Becker 1984; Mereghetti et al. 1996) demonstrates that the SNR resulted from the core-collapse of a massive star. These stars have powerful winds that can result in substantial mass loss well before the supernova explosion, and which can extend for many parsecs from the star (Lozinskaya 1992; García-Segura et al. 1996a,b) It is thus both theoretically expected and well-established from observations that many SNRs are propagating through their progenitor stellar winds, with consequent implications for an SNR’s dynamics and emission properties (Chevalier 1982; Chevalier & Liang 1989; Dwarkadas 2007; Weiler et al. ???). Indeed, such a possibility has been specifically suggested for G296.5+10.0 by Storey et al. (1992), to explain the high degree of mirror symmetry between the two limbs.

It is also well-established that at least some massive stars harbor strong magnetic fields (e.g. Wade 2003), and that these stars correspondingly launch magnetized winds (Weber & Davis 1967; Ignace et al. 1998; ud-Doula & Owocki 2002). The effects on an SNR expanding into a magnetized wind were discussed by Chevalier & Luo (1994), but the resulting RM of the swept-up wind was not addressed. Here we provide a first simple calculation of the likely Faraday rotation signature of this interaction; a subsequent study will further explore this phenomenon through a detailed magnetohydrodynamical calculation.

As noted above, an azimuthal magnetic field naturally produces Faraday rotation that is positive on one side of the center and negative on the other. For this field to have been produced by the stellar wind of the progenitor, we need to assume that the symmetry axis of the SNR corresponds to the spin-axis of the progenitor (see Storey et al. 1992) and that the field pattern in the wind is preserved when it is swept up by the SNR.

However, we note that the simplest geometry for a magnetized stellar wind is a split monopole, in which the magnetic field configurations in the northern and southern hemispheres have opposite polarities, separated by a current sheet (Sakurai 1985; Mestel 2003). For such a wind, the azimuthal component of the pre-supernova magnetic field will be directed in opposite directions above and below the equatorial plane of the progenitor. The simplistic expectation is that a swept-up shell of such material would show a quadrupolar

pattern of RMs with, for example, positive RMs to the northwest and southeast, and negative RMs to the northeast and southwest. This is not the pattern that we observe in Figure 1.

For a magnetized swept-up wind to be a viable explanation of the observed RMs, we thus require a higher-order field in the progenitor wind, such as an aligned quadrupole. Such a wind, as may occur in at least some supernova progenitors (Thompson & Landstreet 1985), can have an azimuthal field of one polarity in a broad equatorial region covering both northern and southern sides of the equatorial plane, with regions of alternating polarity toward the poles. Since the barrel morphology of SNR G296.5+10.0 is dominated by two limbs on either side of the symmetry axis, this is a geometry that can potentially match the observed RM pattern. Further investigations of this wind geometry and its interaction with a SNR shock are needed, but for the purposes of the discussion below, we assume that this or other simple wind patterns can produce the RMs seen in our data, and we now consider whether the magnitudes of the RMs are consistent with expectations from a swept-up stellar wind.

For a spherical stellar wind of mass-loss rate  $\dot{M}$  and asymptotic velocity  $V_\infty$ , conservation of mass implies that the number density  $n(r)$  of gas at a radius  $r$  from the center of the star (where  $r$  lies outside the wind acceleration region) is:

$$n(r) = \frac{\dot{M}}{4\pi r^2 V_\infty m_H}, \quad (2)$$

where  $m_H$  is the mass of a hydrogen atom.

For a rotating star with a magnetic field, the (presumed ionized) stellar wind is channeled by the magnetic field lines i.e. the plasma is frozen into the field. Magnetic field lines leave the surface of the star radially and rapidly wind up into a spiral shape at radii greater than the maximum radius of co-rotation. For a star of radius  $R_*$  with an equatorial rotational velocity  $V_{rot}$  and assuming symmetry above and below the equatorial plane, the strength,  $B_\phi(r)$ , of the azimuthal component of the stellar wind’s magnetic field (Lamers & Cassinelli 1999) is:

$$B_\phi(r) = B_* \left( \frac{R_*}{r} \right) \left( \frac{V_{rot}}{V_\infty} \right), \quad (3)$$

for  $r \gg R_*$ , where  $B_*$  is the magnetic field strength at  $r = R_*$ .

We now consider the result of an SNR expanding through this wind, so that the gas and magnetic field distributions described by these equations are swept up into a thin shell of radius  $R$  and thickness  $\Delta R$ . For the purposes of the present discussion, we make the simplifying assumption that after this material is swept up, the shocked material within the shell has a uniform density  $n_1$  and a uniform magnetic field strength  $B_1$ , as for the simpler case discussed in §4.3 above.

The total number of atoms in the wind,  $N_{tot}$ , swept up by the SNR is:

$$N_{tot} = \int_{R_*}^R n(r) 4\pi r^2 dr = \frac{\dot{M}R}{V_\infty m_H} \quad (4)$$

for  $r \gg R_*$ .

Conservation of mass requires that  $N_{tot} = 4\pi R^2 \Delta R n_1$ , so that:

$$n_1 = \frac{\dot{M}}{4\pi R^2 V_\infty m_H} \left( \frac{R}{\Delta R} \right) = n(R) \left( \frac{R}{\Delta R} \right). \quad (5)$$

We can similarly consider the total magnetic flux,  $\Phi_{tot}$ , passing through a meridional (constant  $\Phi$ ) area element that extends in radius from  $R_*$  to  $R$  and spans  $\Delta\psi$  in colatitude:

$$\Phi_{tot} = \int_{R_*}^R B_\phi(r) r dr = B_* R_* R \Delta\psi \left( \frac{V_{rot}}{V_\infty} \right). \quad (6)$$

where  $\psi$  is the polar angle of the spherical co-ordinate system.

As the material is ejected radially, the meridional area is radially compressed but the polar angle is unchanged before and after the compression.

Assuming conservation of flux after the SNR sweeps up this material, we require  $\Phi_{tot} = B_1 R \Delta R \Delta\psi$  and hence:

$$B_{\phi,1} = B_* \left( \frac{R_*}{\Delta R} \right) \left( \frac{V_{rot}}{V_\infty} \right) = B_\phi(R) \left( \frac{R}{\Delta R} \right). \quad (7)$$

We are now in a position to estimate the RM produced by the swept-up wind,

$$\text{RM}_{\text{wind}} = 0.81 \int \left( \frac{n_1}{\text{cm}^{-3}} \right) \left( \frac{B_{\phi,1}}{\mu\text{G}} \right) \left( \frac{dl}{\text{pc}} \right) \cos\theta \text{ rad m}^{-2} \quad (8)$$

where the integral is along a path-length  $dl$  through the shell,  $\theta$  is the angle of  $B_1$  to the line of sight, and where we have assumed that the swept-up wind is fully ionized. As in §4.3, the maximum path length through the limb is  $L \approx 2(2R\Delta R)^{1/2}$ . Through the limbs of the SNR, a swept-up azimuthal field will be oriented such that  $\theta \approx 0$ . Substituting Equations (5) and (7) into Equation (8), and writing  $x = V_{rot}/V_\infty$ , we derive:

$$\text{RM}_{\text{wind}} = 3.6 \times 10^{-6} \left( \frac{R}{\Delta R} \right)^{3/2} \left( \frac{B_*}{\text{G}} \right) \left( \frac{R_*}{100R_\odot} \right) \left( \frac{x}{0.1} \right) \left( \frac{\dot{M}}{10^{-6}M_\odot \text{ yr}^{-1}} \right) \left( \frac{R}{20 \text{ pc}} \right)^{-2} \left( \frac{V_\infty}{1000 \text{ km s}^{-1}} \right)^{-1} \text{ rad m}^{-2}. \quad (9)$$

This equation clearly implies that a wind from a main-sequence or Wolf-Rayet supernova progenitor will not produce significant Faraday rotation when it is swept up, because the stellar radius is small ( $\leq 10R_\odot$ ), the mass-loss rate is low ( $\dot{M} < 10^{-5} - 10^{-6}M_\odot \text{ yr}^{-1}$ ) and the wind velocity is high ( $V_\infty > 1000 \text{ km s}^{-1}$ ) (see Chevalier & Liang 1989; Dwarkadas 2007; Crowther 2007, and references therein). However, if we adopt representative values for a red supergiant and its wind,  $B_* = 500 \text{ G}$ ,  $R_* = 300R_\odot$ ,  $x = 0.1$ ,  $\dot{M} = 1 \times 10^{-5}M_\odot \text{ yr}^{-1}$  and  $V_\infty = 30 \text{ km s}^{-1}$  (Gray & Toner 1987; Dorsch 2004; Vlemmings et al. 2005; van Belle et al. 2009; van Loon 2009), we predict:

$$\text{RM}_{\text{wind}} = 1.8 \left( \frac{R}{\Delta R} \right)^{3/2} \text{ rad m}^{-2}, \quad (10)$$

For a shell thickness  $R/\Delta R \approx 8$  as indicated by the radio morphology of the SNR, this yields  $\text{RM}_{\text{wind}} \approx 40 \text{ rad m}^{-2}$ , which is a factor of two larger than the observed RM, as required (see discussion about Faraday depth effects in §4.3). We note that a red supergiant wind flowing outward for  $\sim 1 \text{ Myr}$  (e.g. Woosley et al. 2002) at  $V_\infty \approx 30 \text{ km s}^{-1}$  will extend  $\sim 30 \text{ pc}$  from the star, so that an SNR with a current radius  $R \approx 20 \text{ pc}$  would still be propagating through this wind.

We caution that Equation (9) has many free parameters, and that supernova progenitors show a very wide range of properties. Thus we cannot conclusively demonstrate or rule out that the RM seen against the SNR matches the expected Faraday rotation from its progenitor wind. However, having ruled out other reasonable alternatives for the observed RM pattern in §§4.2 & 4.3, and having shown that the RM for at least one set of reasonable wind parameters can match the observations, we conclude that an azimuthal magnetic field in the stellar wind of a red supergiant progenitor can potentially explain both the sign and magnitude of the RMs seen against SNR G296.5+10.0.

As an additional test for this scenario of a swept-up red supergiant wind, we now consider whether the barrel-shape of G296.5+10.0 is consistent with our proposed model. In order to do this, we will examine the two possible mechanisms by which a magnetized red supergiant progenitor star can produce a bilateral SNR. These are: (i) expansion of the supernova into a magnetized stellar wind and (ii) expansion of the supernova into a stellar wind with a biconical outflow aligned with the spin axis (Manchester 1987).

In the first case, the circumstellar material is distributed axisymmetrically by the action of the magnetic field (Sakurai 1985) and is swept up by the expanding supernova shock into a barrel-shaped SNR. Similarly, in the second case the supernova sweeps up material in all directions *except* for a bipolar outflow cavity, which has been largely evacuated of material due to the high wind velocity along this axis. Under either of these schemes, the result is a remnant with two bright limbs (one at either side of the spin axis of the star) and two null

points along the axis.

These two models for the creation of barrel-shaped SNRs both involve a supernova expanding through an axisymmetric distribution of circumstellar material. A prominent example of such a system is the young barrel-shaped supernova remnant of SN1987A. This remnant is understood to have been shaped by the interaction of the supernova shock with the anisotropic circumstellar medium caused by the red and blue supergiant phases of the progenitor star (Dwarkadas 2007). We argue that a supernova expanding into a magnetically-driven stellar wind is the most plausible scenario and explains the structure of G296.5+10.0. This notion is supported by the findings of Storey et al. (1992), who argued that the small-scale correlations in structure on either side of the SNR originate from changes in the outflow from the progenitor star rather than an external ISM.

An additional consideration is the large axial ratio of SNR G296.5+10.0. Although Roger et al. (1988) attributed the elongation of the limbs to coupling of material with the magnetic field of the ambient ISM, a model involving a SNR expanding into a magnetized stellar wind can just as readily explain this phenomenon. The distribution of circumstellar material resulting from a magnetized progenitor stellar wind will result in a large fraction of material being deposited in the magnetic equatorial plane and progressively less mass distributed towards the polar regions. A spherically symmetric supernova explosion occurring within such a medium will result in a remnant with some ‘straightening’ of the limbs, because when the shell is being swept up, the pressure experienced by the SNR shell encountering the equatorial CSM will be greater than the pressure encountered by that part encountering less dense material towards the polar regions (Blondin et al. 1996). This picture is consistent with the small-scale structure symmetry noted by Storey et al. (1992) in G296.5+10.0.

A final piece of the puzzle is the radio polarization observation of SNR G296.5+10.0 by Milne & Haynes (1994). By observing at higher radio frequencies than we present here, they were able to infer the intrinsic orientation of the polarization vectors in the SNR’s synchrotron radiation, before this emission is Faraday rotated in foreground thermal gas. They found that the magnetic field orientation of the synchrotron-emitting regions has a projection on the sky which is largely tangential to the rim of the SNR. This can be explained in the context of a magnetized progenitor wind if we consider a progenitor star with its spin axis tilted with respect to the plane of the sky and with an azimuthal magnetic field. Such an alignment would produce a supernova remnant with linearly polarized emission that is aligned with the sky-plane magnetic field direction tangential to the remnant limbs, as well as a line-of-sight magnetic field that reversed direction between the two separate limbs, as observed from our Faraday rotation measurements.

## 5. Conclusions

Using rotation measure synthesis, we have made Faraday rotation maps of the supernova remnant G296.5+10.0. The limbs of the remnant were found to have RMs of opposite signs and separated by approximately  $40 \text{ rad m}^{-2}$ , implying that the magnetic field in the foreground to the polarized SNR emission is oriented in opposite directions on either side of the SNR’s symmetry axis. By comparing the published RMs of pulsars observed through similar sight-lines through the Galaxy, we demonstrated that the spread of RMs within the remnant is inconsistent with Faraday rotation by the foreground magneto-ionized medium. We also considered whether a swept-up ambient interstellar medium can explain the RM distribution in G296.5+10.0, but found a large discrepancy between the observed rotation measures and those predicted by theory. Finally, we found that the swept-up wind of a red supergiant progenitor star could explain the observed magnitude and distribution of RMs in the remnant, as well as the linear polarization found by other authors. This would require an aligned quadropole or similar magnetic field morphology in the wind of the progenitor star.

Future observational studies should use RM synthesis to map Faraday rotation in a larger sample of Galactic supernova remnants. Focusing on remnants that lie at relatively large Galactic latitudes will minimize the effect of the Galactic foreground and enable an accurate determination of the intrinsic properties of the magnetized plasma within the remnants. If similar morphologies are found, we will be able to gain a deeper understanding about the mass-loss histories of progenitor stars prior to their supernova events. If the Faraday rotation in the remnant represents the signature of a magnetized stellar wind, then the method suggested by Kothes & Brown (2009) for studying ambient magnetic fields in the Galaxy using SNRs is not only a powerful *in situ* probe of magnetic fields, but also of SNR progenitor winds. By studying a larger sample of sources we can hope to understand the physical origin of magnetic fields swept up in supernova remnants. In parallel, magnetohydrodynamical simulations of red supergiant winds should also be employed to test the validity of our model of a swept-up magnetized stellar wind in G296.5+10.0.

We gratefully acknowledge Stan Owocki, Asif ud-Doula and Wouter Vlemmings for helpful discussions on magnetic fields in massive stars and their winds. The Australia Telescope is funded by the Commonwealth of Australia for operation as a National Facility managed by CSIRO. L.H-S. and B.M.G. acknowledge the support of the Australian Research Council through grants FF0561298 and DP0986386.

*Facilities:* ATCA



## REFERENCES

- Bisnovatyi-Kogan, G. S., Lozinskaia, T. A., & Silich, S. A. 1990, *Ap&SS*, 166, 277
- Blondin, J. M., Lundqvist, P., & Chevalier, R. A. 1996, *ApJ*, 472, 257
- Brentjens, M. A. & de Bruyn, A. G. 2005, *A&A*, 441, 1217
- Brentjens, M. A. & de Bruyn, A. G. 2005, *A&A*, 441, 1217
- Brown, J. C., Haverkorn, M., Gaensler, B. M., Taylor, A. R., Bizunok, N. S., McClure-Griffiths, N. M., Dickey, J. M., & Green, A. J. 2007, *ApJ*, 663, 258
- Brown, J. C. & Taylor, A. R. 2001, *ApJ*, 563, L31
- Burton, M. G., Geballe, T. R., Brand, P. W. J. L., & Webster, A. S. 1988, *MNRAS*, 231, 617
- Caswell, J. L., McClure-Griffiths, N. M., & Cheung, M. C. M. 2004, *MNRAS*, 352, 1405
- Chevalier, R. A. 1974, *ApJ*, 188, 501
- . 1982, *ApJ*, 259, L85
- Chevalier, R. A. 1982, *ApJ*, 258, 790
- . 1999, *ApJ*, 511, 798
- Chevalier, R. A. & Fransson, C. 1987, *Nature*, 328, 44
- Chevalier, R. A. & Liang, E. P. 1989, *ApJ*, 344, 332
- Chevalier, R. A. & Luo, D. 1994, *ApJ*, 421, 225
- Chevalier, R. A. & Oishi, J. 2003, *ApJ*, 593, L23
- Claussen, M. J., Frail, D. A., Goss, W. M., & Gaume, R. A. 1997, *ApJ*, 489, 143
- Cordes, J. M. & Lazio, T. J. W. 2002, preprint (arXiv:astro-ph/0207156)
- Crowther, P. A. 2007, *Ann. Rev. Astr. Ap.*, 45, 177
- Dickel, J. R. & Milne, D. K. 1976, *Aust. J. Phys.*, 29, 435
- Dorsch, S. B. F. 2004, *A&A*, 423, 1101
- Dubner, G. M., Colomb, F. R., & Giacani, E. B. 1986, *AJ*, 91, 343

- Dwarkadas, V. V. 2005, *ApJ*, 630, 892
- Dwarkadas, V. V. 2007, *ApJ*, 667, 226
- Dwarkadas, V. V. 2007, in *American Institute of Physics Conference Series*, Vol. 937, *Supernova 1987A: 20 Years After: Supernovae and Gamma-Ray Bursters*, ed. S. Immler, K. Weiler, & R. McCray, 120–124
- Foster, T., Routledge, D., & Kothes, R. 2004, *A&A*, 417, 79
- Frail, D. A., Goss, W. M., & Slysh, V. I. 1994, *ApJ*, 424, L111
- Franco, J., Tenorio-Tagle, G., Bodenheimer, P., & Rozyczka, M. 1991, *PASP*, 103, 803
- Fukui, Y., Moriguchi, Y., Tamura, K., Yamamoto, H., Tawara, Y., Mizuno, N., Onishi, T., Mizuno, A., Uchiyama, Y., Hiraga, J., Takahashi, T., Yamashita, K., & Ikeuchi, S. 2003, *PASJ*, 55, L61
- Gaensler, B. M. 1998, *ApJ*, 493, 781
- Gaensler, B. M., Manchester, R. N., & Green, A. J. 1998, *MNRAS*, 296, 813
- Gaensler, B. M., Manchester, R. N., Staveley-Smith, L., Tzioumis, A. K., Reynolds, J. E., & Kesteven, M. J. 1997, *ApJ*, 479, 845
- García-Segura, G., Langer, N., & Mac Low, M.-M. 1996a, *A&A*, 316, 133
- García-Segura, G., Mac Low, M.-M., & Langer, N. 1996b, *A&A*, 305, 229
- Gardner, F. F. & Whiteoak, J. B. 1966, *Ann. Rev. Astr. Ap.*, 4, 245
- Giacani, E. B., Dubner, G. M., Green, A. J., Goss, W. M., & Gaensler, B. M. 2000, *AJ*, 119, 281
- Gray, D. F. & Toner, C. G. 1987, *ApJ*, 322, 360
- Green, A. J., Frail, D. A., Goss, W. M., & Otrupcek, R. 1997, *AJ*, 114, 2058
- Gvaramadze, V. V. 2006, *A&A*, 454, 239
- Heald, G., Braun, R., & Edmonds, R. 2009, *A&A*, 503, 409
- Helfand, D. J. & Becker, R. H. 1984, *Nature*, 307, 215
- Ignace, R., Cassinelli, J. P., & Bjorkman, J. E. 1998, *ApJ*, 505, 910

- Koo, B. & Heiles, C. 1995, *ApJ*, 442, 679
- Kothes, R. & Brown, J. 2009, in *Cosmic Magnetic Fields: From Planets, to Stars and Galaxies (IAU Symposium 259)*, ed. K. G. Strassmeier, A. G. Kosovichev, & J. E. Beckman (Cambridge: Cambridge University Press), 75–80
- Koyama, K., Petre, R., Gotthelf, E. V., Hwang, U., Matsuura, M., Ozaki, M., & Holt, S. S. 1995, *Nature*, 378, 255
- Kulsrud, R. M., Bernstein, I. B., Krusdal, M., Fanucci, J., & Ness, N. 1965, *ApJ*, 142, 491
- Lamers, H. J. G. L. M. & Cassinelli, J. P. 1999, *Introduction to Stellar Winds* (Cambridge: Cambridge University Press)
- Landecker, T. L., Routledge, D., Reynolds, S. P., Smegal, R. J., Borkowski, K. J., & Seward, F. D. 1999, *ApJ*, 527, 866
- Lozinskaya, T. A. 1992, *Supernovae and Stellar Wind in the Interstellar Medium* (New York: American Institute of Physics)
- Manchester, R. N. 1987, *A&A*, 171, 205
- Manchester, R. N., Hobbs, G. B., Teoh, A., & Hobbs, M. 2005, *AJ*, 129, 1993
- Matsui, Y., Long, K. S., Dickel, J. R., & Greisen, E. W. 1984, *ApJ*, 287, 295
- Matsui, Y., Long, K. S., & Tuohy, I. R. 1988, *ApJ*, 329, 838
- Mereghetti, S., Bignami, G. F., & Caraveo, P. A. 1996, *ApJ*, 464, 842
- Mestel, L. 2003, *Stellar Magnetism* (Oxford: Oxford University Press)
- Milne, D. K. & Haynes, R. F. 1994, *MNRAS*, 270, 106
- Noutsos, A., Johnston, S., Kramer, M., & Karastergiou, A. 2008, *MNRAS*, 386, 1881
- Pacholczyk, A. G. 1970, *Radio Astrophysics* (San Francisco: Freeman)
- Pineault, S., Landecker, T. L., Madore, B., & Gaumont-Guay, S. 1993, *AJ*, 105, 1060
- Qiao, G. J., Manchester, R. N., Lyne, A. G., & Gould, D. M. 1995, *MNRAS*, 274, 572
- Roger, R. S., Milne, D. K., Kesteven, M. J., Wellington, K. J., & Haynes, R. F. 1988, *ApJ*, 332, 940

- Sakurai, T. 1985, *A&A*, 152, 121
- Sault, R. J., Bock, D. C.-J., & Duncan, A. R. 1999, *A&AS*, 139, 387
- Sault, R. J. & Killeen, N. E. B. 2004, *The Miriad User's Guide* (Sydney: Australia Telescope National Facility), (<http://www.atnf.csiro.au/computing/software/miriad/>)
- Sokoloff, D. D., Bykov, A. A., Shukurov, A., Berkhuijsen, E. M., Beck, R., & Poezd, A. D. 1998, *MNRAS*, 299, 189
- Storey, M. C., Staveley-Smith, L., Manchester, R. N., & Kesteven, M. J. 1992, *A&A*, 265, 752
- Storey, M. C., Staveley-Smith, L., Manchester, R. N., & Kesteven, M. J. 1992, *A&A*, 265, 752
- Tanimori, T., Hayami, Y., Kamei, S., Dazeley, S. A., Edwards, P. G., Gunji, S., Hara, S., Hara, T., Holder, J., Kawachi, A., Kifune, T., Kita, R., Konishi, T., Masaïke, A., Matsubara, Y., Matsuoka, T., Mizumoto, Y., Mori, M., Moriya, M., Muraishi, H., Muraki, Y., Naito, T., Nishijima, K., Oda, S., Ogió, S., Patterson, J. R., Roberts, M. D., Rowell, G. P., Sakurazawa, K., Sako, T., Sato, Y., Susukita, R., Suzuki, A., Suzuki, R., Tamura, T., Thornton, G. J., Yanagita, S., Yoshida, T., & Yoshikoshi, T. 1998, *ApJ*, 497, L25
- Thompson, I. B. & Landstreet, J. D. 1985, *ApJ*, 289, L9
- Tian, W. W. & Leahy, D. A. 2008, *MNRAS*, 391, L54
- ud-Doula, A. & Owocki, S. P. 2002, *ApJ*, 576, 413
- ud-Doula, A., Owocki, S. P., & Townsend, R. H. D. 2008, *MNRAS*, 385, 97
- van Belle, G. T., J., C.-E. M., & Hart, A. 2009, *MNRAS*, 394, 1925
- van der Laan, H. 1962a, *MNRAS*, 124, 125
- . 1962b, *MNRAS*, 124, 179
- van Loon, J. T. 2009, in *Hot and Cool: Bridging Gaps in Massive Star Evolution*, ed. C. Leitherer, P. D. Bennett, P. W. Morris, & J. T. van Loon (San Francisco: Astronomical Society of the Pacific), in press (arXiv:0906.485)
- Velázquez, P. F., Dubner, G. M., Goss, W. M., & Green, A. J. 2002, *AJ*, 124, 2145

- Vink, J., Bloemen, H., Kaastra, J. S., & Bleeker, J. A. M. 1998, *A&A*, 339, 201
- Vlemmings, W. H. T., van Langevelde, H. J., & Diamond, P. J. 2005, *Mem. della Soc. Ast. It.*, 76, 462
- Wade, G. A. 2003, in *Astronomical Society of the Pacific Conference Series*, Vol. 305, *Astronomical Society of the Pacific Conference Series*, ed. L. A. Balona, H. F. Henrichs, & R. Medupe (San Francisco: Astronomical Society of the Pacific), 16
- Weber, E. J. & Davis, Jr., L. 1967, *ApJ*, 148, 217
- Weiler, K. W., Panagia, N., Sramek, R. A., Van Dyk, S. D., Williams, C. L., Stockdale, C. J., & Kelley, M. T. ????, 258–263
- Whiteoak, J. B. & Gardner, F. F. 1968, *ApJ*, 154, 807
- Woosley, S. E., Heger, A., & Weaver, T. A. 2002, *Rev. Mod. Phys.*, 74, 1015
- Zavlin, V. E., Pavlov, G. G., & Sanwal, D. 2004, *ApJ*, 606, 444
- Zavlin, V. E., Pavlov, G. G., Sanwal, D., & Trümper, J. 2000, *ApJ*, 540, L25

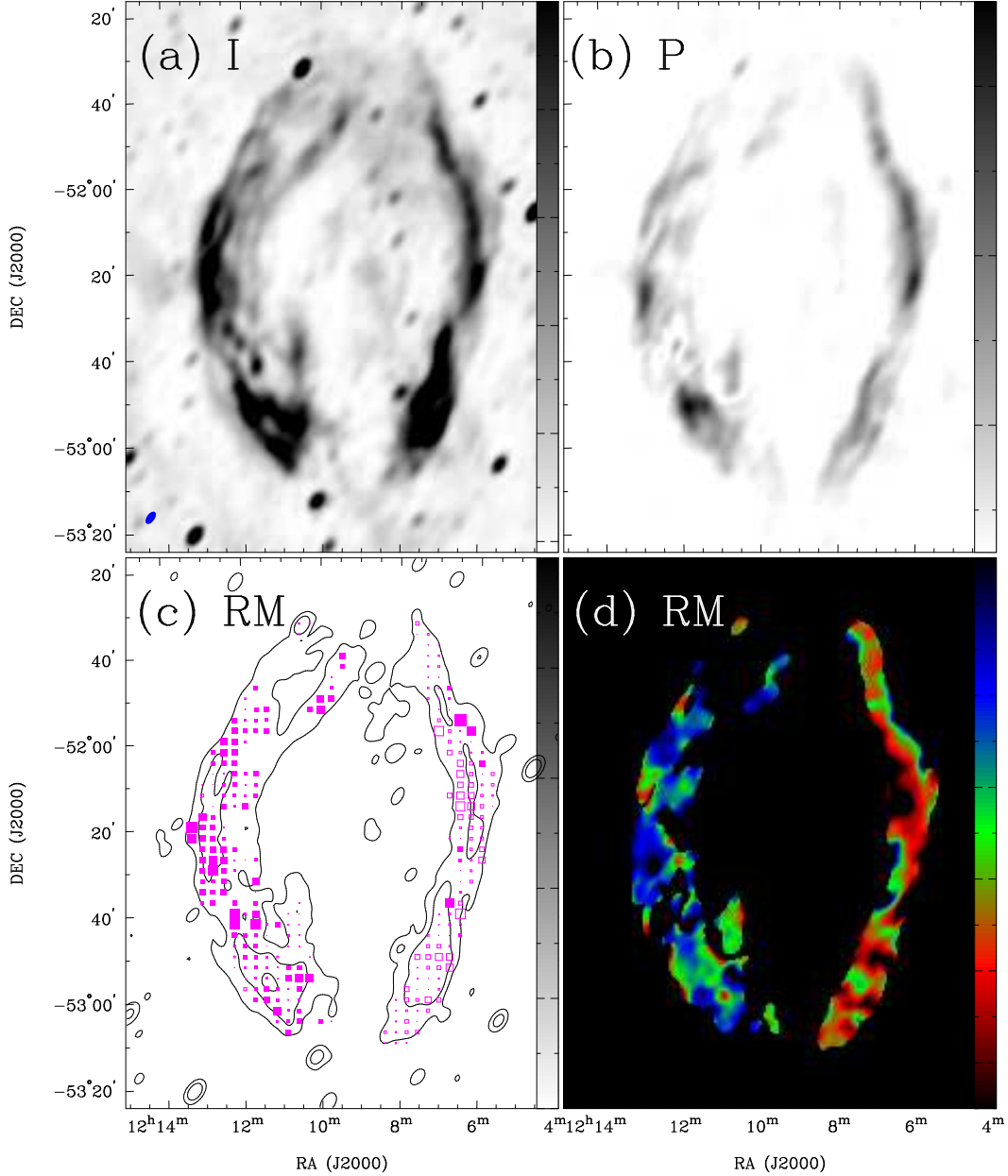


Fig. 1.— ATCA images of SNR G296.5+10.0 at 1.4 GHz. (a) Total intensity, shown with a greyscale ranging between  $-2$  and  $+100$   $\text{mJy beam}^{-1}$ . The blue ellipse at the lower left is the angular resolution of the image,  $3.3 \times 1.8$ , at a position angle of  $-142^\circ$  north through east; (b) Linearly polarized intensity, with greyscale ranging between  $0.5$  and  $70$   $\text{mJy beam}^{-1}$ ; (c) Rotation measure plotted every five pixels ( $150''$ ), with filled boxes representing positive RMs and unfilled boxes representing negative RMs. The linear dimensions of each box indicate the magnitude of the rotation measure. The range of box sizes corresponds to  $|\text{RM}|$  ranging from  $0$  to  $128$   $\text{rad m}^{-2}$ . Contours are the Stokes- $I$  image at  $+20$  and  $+80$   $\text{mJy beam}^{-1}$ ; (d) An image of RM, with the color scale indicating RMs between  $-50$   $\text{rad m}^{-2}$  (red) and  $+70$   $\text{rad m}^{-2}$  (blue) as indicated to the right of the image.

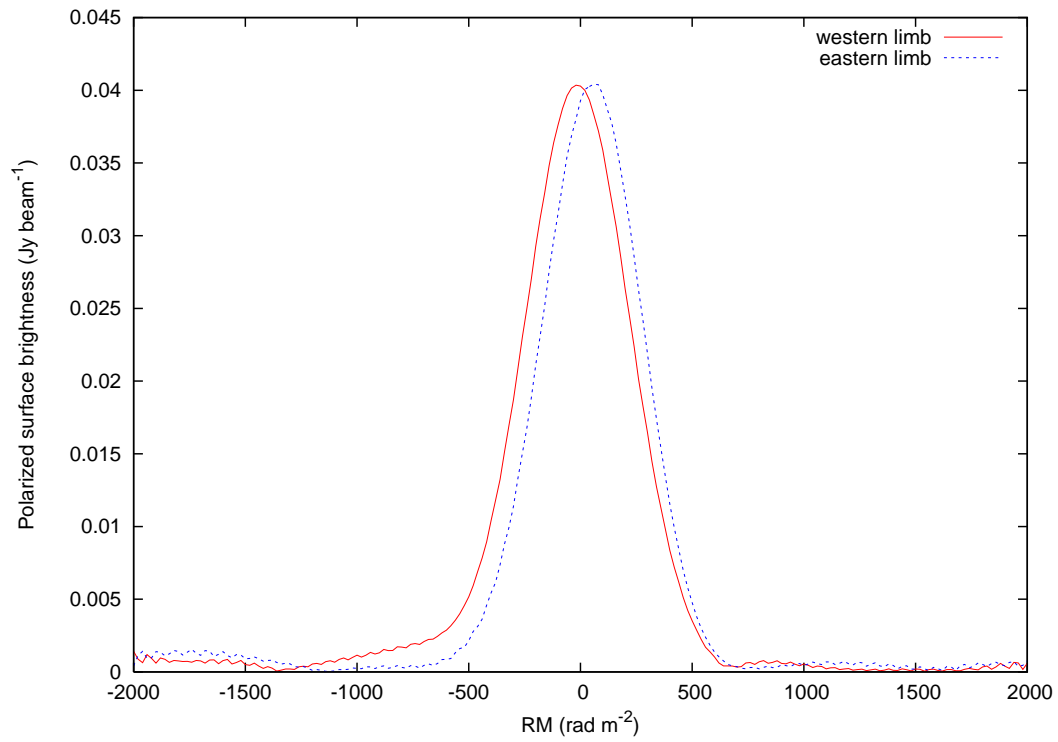


Fig. 2.— The RM synthesis spectra of representative pixels in the eastern (blue) and western (red) limbs of SNR G296.5+10.0. Spectral deconvolution has been applied to remove the sidelobes caused by incomplete sampling in  $\lambda^2$  space.

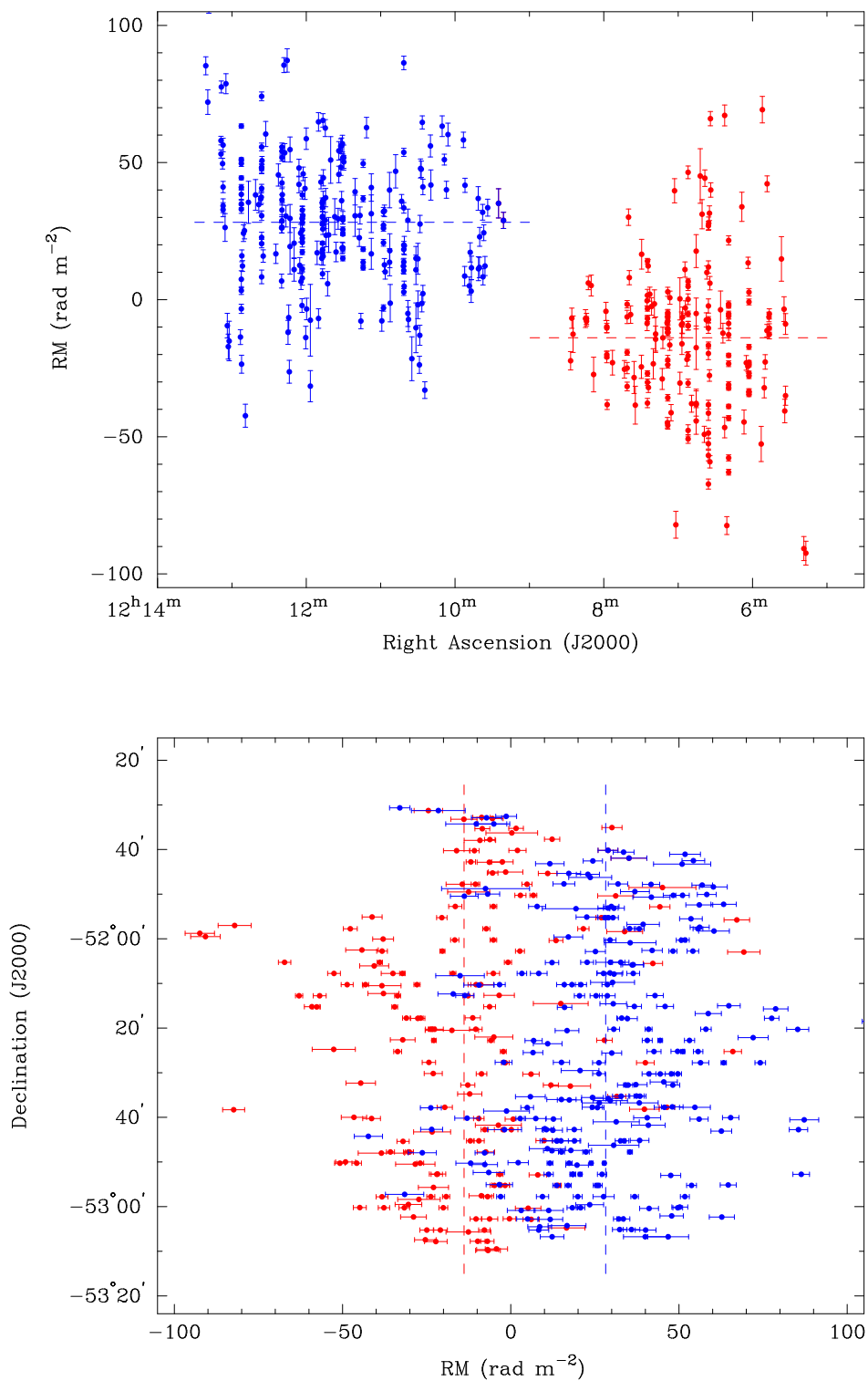


Fig. 3.— Plots of RM against right ascension (top) and against declination (bottom) in G296.5+10.0 for the RM distribution in Figure 1 (c); red points are in the western limb and blue points are in the eastern limb. The mean RM for each limb is displayed as a dashed line.